doi:10.1093/brain/aww130 BRAIN 2016: 139; 2143–2153 | 2143

BRAIN
A JOURNAL OF NEUROLOGY

Identification of mutations in the *MYO9A* gene in patients with congenital myasthenic syndrome

Emily O'Connor,[1]* Ana Töpf,[1]* Juliane S. Müller,[2] Daniel Cox,[1] Teresinha Evangelista,[1] Jaume Colomer,[3] Angela Abicht,[4] Jan Senderek,[4] Oswald Hasselmann,[5] Ahmet Yaramis,[6] Steven H. Laval[1] and Hanns Lochmüller[1]

*These authors contributed equally to this work.

Congenital myasthenic syndromes are a group of rare and genetically heterogenous disorders resulting from defects in the structure and function of the neuromuscular junction. Patients with congenital myasthenic syndrome exhibit fatigable muscle weakness with a variety of accompanying phenotypes depending on the protein affected. A cohort of patients with a clinical diagnosis of congenital myasthenic syndrome that lacked a genetic diagnosis underwent whole exome sequencing in order to identify genetic causation. Missense biallelic mutations in the *MYO9A* gene, encoding an unconventional myosin, were identified in two unrelated families. Depletion of MYO9A in NSC-34 cells revealed a direct effect of MYO9A on neuronal branching and axon guidance. Morpholino-mediated knockdown of the two *MYO9A* orthologues in zebrafish, *myo9aa/ab*, demonstrated a requirement for MYO9A in the formation of the neuromuscular junction during development. The morphants displayed shortened and abnormally branched motor axons, lack of movement within the chorion and abnormal swimming in response to tactile stimulation. We therefore conclude that MYO9A deficiency may affect the presynaptic motor axon, manifesting in congenital myasthenic syndrome. These results highlight the involvement of unconventional myosins in motor axon functionality, as well as the need to look outside traditional neuromuscular junction-specific proteins for further congenital myasthenic syndrome candidate genes.

1 John Walton Muscular Dystrophy Research Centre, MRC Centre for Neuromuscular Diseases, Institute of Genetic Medicine, Newcastle University, Newcastle upon Tyne, NE1 3BZ, UK
2 Wellcome Trust Centre for Mitochondrial Research, Institute of Genetic Medicine, Newcastle University, Newcastle upon Tyne, UK
3 Neuromuscular Unit, Neurology Department, Fundación Sant Joan de Déu, Hospital Materno-Infantil Sant Joan de Déu, Passeig Sant Joan de Déu, 2, 08950 Esplugues de Llobregat, Barcelona, Spain
4 Friedrich-Baur-Institute, Ludwig-Maximilians-University, 80336 Munich, Germany
5 Children's Hospital of Eastern Switzerland, Department of Neuropediatrics, Claudiusstrasse 6, 9006 St. Gallen, Switzerland
6 Paediatric Neurology Unit, Diyarbakır Memorial Hospital, Turkey

Correspondence to: Hanns Lochmüller,
The John Walton Muscular Dystrophy Research Centre,
MRC Centre for Neuromuscular Diseases, Institute of Genetic Medicine,
Newcastle University, Central Parkway,
Newcastle upon Tyne, NE1 3BZ, UK
E-mail: Hanns.Lochmuller@ncl.ac.uk

Keywords: congenital myasthenic syndrome; neuromuscular junction; MYO9A; unconventional myosin; whole exome sequencing

Abbreviations: CMS = congenital myasthenic syndrome; NMJ = neuromuscular junction

Received September 1, 2015. Revised March 29, 2016. Accepted April 20, 2016. Advance Access publication June 3, 2016

Introduction

The vertebrate neuromuscular junction (NMJ) is a highly specialized cholinergic synapse, critical for the initiation of nerve-evoked muscle contractions by means of signal transmission from the presynaptic motor axons to the postsynaptic muscle fibres. Due to the highly organized and structured nature of the NMJ, loss or dysregulation of one of a number of proteins can affect synaptic function leading to congenital myasthenic syndrome (CMS), a group of rare, genetically heterogeneous disorders (Cruz *et al.*, 2014). CMS is characterized by fatigable muscle weakness, commonly affecting facial muscles, including muscles that control the eyelids and move the eyes, as well as those involved in chewing and swallowing. However, diagnosis of CMS is only confirmed upon detection of abnormal jitter on single fibre EMG and/or decrement in repetitive nerve stimulation, indicating dysfunction of the NMJ transmission. To date, in excess of 20 causative genes have been reported for CMS. These only rarely affect the pre-synaptic NMJ, such as choline acetyltransferase mutations, or the synaptic cleft, by disrupting COLQ, but mainly affect proteins of the post-synaptic NMJ, including the subunits of acetylcholine receptors (Cruz *et al.*, 2014). Despite the number of genes identified, ~20% of individuals with a clinical diagnosis of CMS are lacking a genetic diagnosis, indicating that there are still a number of causative genes to be identified (Finlayson *et al.*, 2013).

The use of whole-exome sequencing to identify novel causative variants and genes remains an invaluable method for the successful diagnosis and treatment of these individuals. Here, we have identified compound heterozygous and homozygous variants in an unconventional myosin gene, *MYO9A* in two unrelated CMS families.

Unconventional myosins form a subset of the myosin family of molecular motors that have the ability to bind to actin filaments and move relative to the actin cytoskeleton of cells. They are expressed in neurons of the peripheral nervous system, and have been shown to play an important role in axonal transport (Bridgman, 2009). Unconventional myosins are composed of three distinct regions: the head region, which is able to bind actin filaments, hydrolyse ATP and generate force; the neck region, which contains a varying number of IQ motifs for the binding of light chains such as calmodulin; and the tail region, which is highly divergent, conveying functions specific to each class (Hartman *et al.*, 2011). Thus far unconventional myosins have been associated with Usher syndrome (mutations in *MYO7A*) (Well *et al.*, 1995) and Griscelli syndrome (mutations in *MYO5A*) (Pastural *et al.*, 1997). MYO9A maintains the features of typical myosins including the myosin motor domain (Fig. 1A); however, it acts as a single headed processive motor and has a tail region containing a Rho-GTPase domain, through which MYO9A can inhibit RHOA by stimulating its GTPase activity (Liao *et al.*, 2010). Following the identification of mutations in the *MYO9A* gene in three patients with CMS, analysis of MYO9A localization and function *in vitro* and *in vivo* offers preliminary evidence for a role of the protein at the NMJ.

Materials and methods

Patients

Patient 1 is the first daughter of healthy non-consanguineous parents of German origin (Fig. 1B). She was referred to paediatric neurology due to swallowing difficulties, proximal and

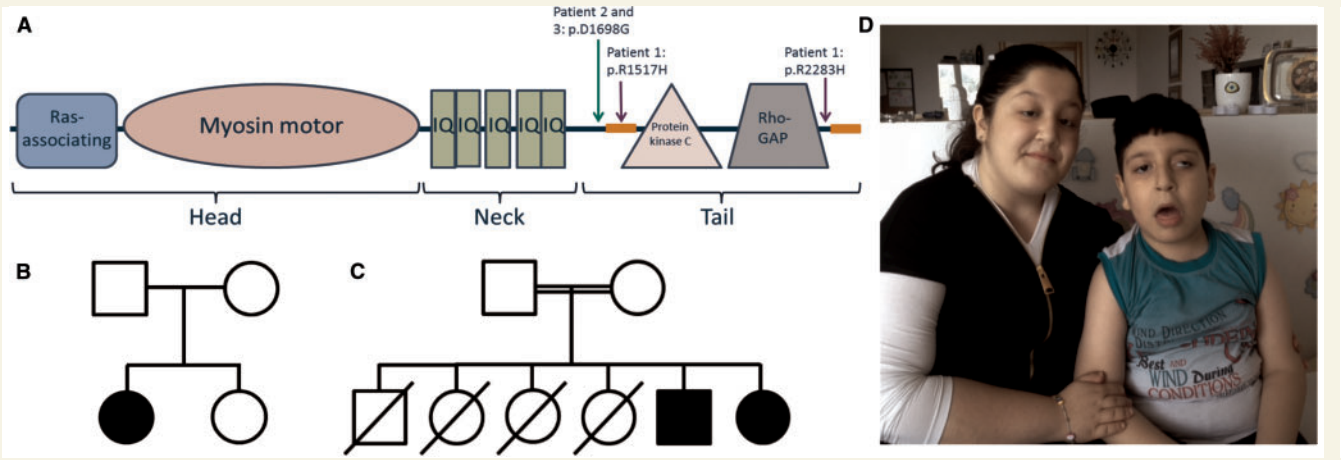

Figure 1 Structure of MYO9A and patient pedigrees. (**A**) Diagram depicting the structure of MYO9A and the protein position of the variants identified in Patients 1–3. Sequences before and after the Rho-GTPase domain are predicted to adopt a coiled coil structure (Gorman *et al.*, 1999), represented by orange boxes. Accession number: NM_006901, Transcript: ENST00000356056. (**B**) Pedigree for Patient 1. (**C**) Pedigree for Patients 2 and 3. (**D**) Image of Patients 2 and 3 displaying bilateral ptosis and ophthalmoplegia; with asymmetric upward deviation of gaze (left eye) in the male patient.

distal muscle weakness, episodic apnoea, respiratory failure and ptosis, all with neonatal onset. The patient was aged 4 years at last examination and remains dependant on feeding through a percutaneous endoscopic gastrostromy. A diagnosis of CMS was made following the finding of an abnormal jitter on the orbicularis oculi with single fibre EMG; four abnormal pairs were recorded at an average jitter of 75 µs. At a different site of the orbicularis oculi unstable potentials were identified, even when the stimulation intensity was increased. Testing was then ceased due to distress of the infant; however, results are fully compatible with CMS. With concentric needle EMG there was no evidence of active denervation and the motor unit action potentials had normal configuration making reinnervation as an alternative explanation for abnormal jitter very unlikely. Brain MRI did not reveal any pathological findings and metabolic tests including creatine kinase, organic acids in urine, amino acids in serum and acylcarnitines in blood were all normal. While not yet objectively tested, cognitive function may be slightly delayed. The patient responds positively to a combination of pyridostigmine and 3,4-DAP, showing marked improvements in motor and respiratory function.

Two Kurdish siblings (Fig. 1C), Patients 2 and 3, had prenatal onset of symptoms with reduced foetal movements. At birth Patient 2, who was 5 years of age at last examination, presented with bilateral ptosis and after 2 months showed generalized hypotonia and difficulty with swallowing and chewing. Head control was obtained at 12 months, sitting at 3 years, and walking with support at 5 years of age. Symmetric multivectorial nystagmus, left eye upgaze deviation and ophthalmoplegia are also present (Fig. 1D). Respiratory crises have occurred following oral intake of 3.4-DAP and fluoxetine, as well as during respiratory infection. Patient 2 has also presented with learning difficulties, and has not yet developed the ability to speak. Patient 3, who was 11 years of age at last examination, presented with bilateral ptosis within the first week following birth and in the subsequent few months developed generalized hypotonia, absence of head and truncal control, and difficulty with swallowing and chewing. Sitting was achieved at 12 months, head control at 18 months, and the ability to walk unassisted at 30 months of age. Nystagmus (usually vertical) and oculomotor apraxia with head tilt and symmetric ophthalmoplegia are also present. Episodes of respiratory crises occur during respiratory infection. Brain MRI did not show any pathology. Metabolic testing was normal, including tandem mass spectrometry and creatine kinase in serum, organic acids in urine and amino acids in serum. The diagnosis of CMS was made following the finding of an increased jitter on single fibre EMG in the younger sibling, and a 22% decrement on repetitive nerve stimulation to the right ala nasi muscle in the older sibling. Both patients showed improvement in ptosis, swallowing, chewing and breathing in response to pyridostigmine treatment. The unaffected parents are consanguineous and have previously lost four children during the first year of life, all with respiratory failure, feeding difficulties and hypotonia.

Consent for research was obtained by the referring physicians.

Whole-exome sequencing

Whole-exome sequencing was carried out by deCODE Genetics (Iceland) for Patient 1 and both parents, as well as Patients 2 and 3 and their mother. Exome capture was performed with the 62 Mb Nextera Rapid Capture Expanded Exome kit (Illumina) and sequenced on an Illumina HiSeq 2500 platform. Reads were aligned to the hg19 reference genome using BWA and variants called using GATK. Data for each patient were made available through deCODE's proprietary platform (Clinical Sequence Analyser). Data were then filtered to include only low frequency coding variants present in $\leqslant 1\%$ of the control population, ExAC database (http://exac.broadinstitute.org/), and compatible with an autosomal recessive mode of inheritance as this fits with both pedigrees analysed. Sporadic inheritance was also considered for Patient 1. Only mutations causing moderate [missense and in-frame indels (insertions/deletions)] and high impact (nonsense, frameshifting indels and essential splice sites) effects on the protein structure were included in analysis. Variants were also excluded by manual filtering, including analysis of read depth, alignment of reads and quality of variants by visual inspection. Variants that remained were subjected to segregation analysis using family DNA.

Cell culture

NSC-34 cells were cultured to sub-confluence in Dulbecco's modified Eagle medium (DMEM; Life Technologies) supplemented with 10% foetal bovine serum and 100 units/ml penicillin/streptomycin.

Short hairpin RNA knockdown in NSC-34 cells

Short hairpin (sh)RNA sequences targeting the mouse *Myo9a* gene were designed using the BLOCK-iT™ RNAi Designer (Life Technologies) and cloned into the pSuperior vector (Supplementary Fig. 1). Following transfection, cells were selected using puromycin at 3 µg/ml and cultured for 14 days to confirm stable transfection.

Quantitative real time polymerase chain reaction

To confirm the shRNA-mediated knockdown of *Myo9a* from NSC-34 cells, total RNA from knockdown and control NSC-34 cells was isolated using TRIzol® Reagent (Life Technologies). cDNA was synthesized from isolated RNA by incubation with random primers and SuperScript® III Reverse Transcriptase (Life Technologies) for 2 h at 37°C. Quantitative reverse transcription polymerase chain reaction (qRT-PCR) was performed using a SYBR® Green JumpStart™ Taq ReadyMix according to manufacturer's instructions (Sigma S4438), with primers listed in Supplementary Table 2. Beta-actin was used as an endogenous control, as used elsewhere (Ryan *et al.*, 2009). Three biological replicates in triplicate were run for *Myo9a* and *Actb* (beta-actin), with a corresponding no template control. The relative expression ratio (RER) was determined using the formula:

$$\text{RER of } Myo9a = \frac{2^{-\Delta Ct\text{target(KD}-\text{control)}}}{2^{-\Delta Ct\text{ref(KD}-\text{control)}}}$$

where ΔCt is the difference in crossing points, ref is the corresponding value for the reference gene (*Actb*) and KD refers to the knockdown cells.

Immunofluorescent staining of whole mouse muscle and cells

Mouse lumbrical muscles and NSC-34 cells were fixed in paraformaldehyde (1% and 4%, respectively). Tissue and cells were then permeabilized in 0.1% Triton™ X-100 in PBS, followed by incubation in 4% bovine serum albumin (BSA) in phosphate-buffered saline (PBS) at room temperature. Primary antibodies used are: mouse monoclonal anti-Myosin IXA (1:500, ab76683, Abcam) and rabbit polyclonal anti-synaptophysin (1:100, Fisher Scientific). Secondary antibodies applied are: Alexa Fluor® 488 goat anti-mouse (1:500, Life Technologies), Alexa Fluor® 350 goat anti-rabbit (1:2000, Life Technologies) and Alexa Fluor® 594 goat anti-mouse (1:500, Life Technologies). Direct antibodies used include Alexa Fluor® 594 α-bungarotoxin conjugate (1:1000, Life Technologies) and Oregon Green 488 phalloidin (1:1000, Life Technologies). All antibodies were diluted in 4% BSA in PBS, and washes carried out using PBS, except for α-bungarotoxin, which was diluted in Lilies solution (12 mM $NaHCO_3$, 4 mM KCl, 1 mM KH_2PO_4, 138.8 mM NaCl, 1 mM $MgCl_2$, 2 mM $CaCl_2$, 11 mM glucose). Samples were mounted in Vectashield (Vector Laboratories).

Morpholino knockdown in zebrafish embryos

Interrogation of the UCSC database (Kent *et al.*, 2002; http://genome.ucsc.edu/) revealed two orthologues of *MYO9A* in zebrafish, *myo9aa* and *myo9ab* (ZV9/danRer7 assembly). An antisense morpholino oligonucleotide targeting the splice donor site of exon 4 *myo9aa* and the splice donor site of exon 7 *myo9ab* were designed and synthesized by Gene Tools LLC (USA). A *p53* morpholino oligonucleotide was also purchased and a morpholino oligonucleotide against a human beta-globin mutation was used as a negative control. Sequences are provided in Supplementary Table 1. Knockdown was performed in zygotes of the golden strain (genotype *slc24a5b1/+*) of zebrafish [Zebrafish International Resource Centre (ZIRC)] and Tg(islet-1:GFP) zebrafish (Higashijima *et al.*, 2000). Morpholino oligonucleotide preparation and injection procedure are described in the Supplementary material. At 48 hours post-fertilization (hpf) zebrafish were stimulated on the head or tail with a fine pipette tip to provoke a touch-evoked swim response.

Immunofluorescent staining of whole mount zebrafish

At 48 hpf, injected embryos were dechorionated with Pronase E (Sigma Aldrich) and euthanized by anaesthetic overdose. Whole mount immunofluorescent staining of zebrafish was performed as described previously (Muller *et al.*, 2010). The NMJs were visualized with a mouse anti-SV2 antibody (1:200, Developmental Studies Hybridoma Bank) and Alexa Fluor® 594 α-bungarotoxin conjugate (1:1000, Life Technologies).

Reverse transcription polymerase chain reaction

Total RNA was isolated from 30–40 *myo9aa/myo9ab* morpholino oligonucleotide-injected and non-injected zebrafish embryos at 48 hpf using TRIzol® Reagent (Life Technologies) and cDNA synthesized by incubation with Random Primers (Promega) and dNTPs at 65°C for 5 min, followed by incubation with RNaseOUT™ Recombinant Ribonuclease Inhibitor (Life Technologies) and SuperScript® III Reverse Transcriptase (Life Technologies) according to the manufacturer's instructions. PCR was then performed using the primers listed in Supplementary Table 2.

Microscopy and image analysis

Cells were visualized using an Axio Imager Z1 fluorescent microscope. Whole mouse muscle, knockdown cells and zebrafish were visualized using a Nikon A1R laser scanning confocal microscope. *Z*-stack images of the zebrafish were obtained by scanning one-half of the myotome of the trunk. NSC-34 cells were imaged with a Nikon eclipse TS100 microscope for branch analysis. Images taken with the confocal and Nikon eclipse microscopes were analysed using the NIS-elements AR 4.20.02 software, including NSC-34 cell branching counts and neurite length measurements. Neurites $>20\,\mu m$ length were included in analysis. Islet-1 and golden strain zebrafish were imaged live with a Leica MZ 16 Fluorescent microscope at with an 8× or 4× objective, respectively, and at 24 hpf the number of tail movements within the chorion of the injected and control embryos was assessed in 10 s using a Leica stereomicroscope with a Chameleon digital camera (CMLN-13s2M).

Statistical analysis

The two-sample *t*-test was used to compare the quantity and length of control knockdown and MYO9A knockdown NSC-34 cell neurites, as well as the number of spontaneous movements performed by zebrafish in the chorion at 24 hpf. $P < 0.05$ was taken as statistically significant.

Results

Exome sequencing

Analysis of whole-exome sequencing data for Patient 1 and both of her unaffected parents was carried out and the number of variants identified at each stage of the workflow is shown in Table 1. Segregation analysis by Sanger sequencing of her unaffected sister allowed the exclusion of *TNXB*, leaving only two genes with compound heterozygous variants co-segregating with the disease: *MYO9A* (Fig. 1A) and *AKAP11*. *AKAP11* encodes an A kinase anchor protein, expressed at high levels in spermatogenesis and mature sperm where it is hypothesized to be involved in cell cycle control (Pruitt *et al.*, 2014). *MYO9A* encodes an unconventional myosin protein, part of a family of molecular motors in which members have previously been associated with neuronal growth, and MYO9A in particular with cell migration (Suter *et al.*, 2000; Zhu *et al.*, 2007; Omelchenko, 2012). Although it cannot be ruled out completely, it would seem highly unlikely that mutant AKAP11 causes CMS.

Table 1 The number of variants identified at each stage of the whole exome sequencing analysis workflow for all patients

Patient	Total coding variants	Total autosomal recessive variants	Variants following application of filters	Genes with variants following manual inspection	Genes with variants that segregate
1	13 263	1633	26	*MYO9A* (CHZ) *AKAP11* (CHZ) *TNXB* (CHZ)	*MYO9A* (CHZ) *AKAP11* (CHZ)
2/3	14 065	3265	55	*MYO9A* (Hom) *MAP3K8* (Hom) ADAMTSL3 (Hom) *RYR1* (3 CHZ) *ZNF862* (2 Hom) *CSPP1* (Hom) *CHRNB4* (Hom) *ZNF655* (Hom) *TH* (CHZ) *DNAH11* (CHZ)	*MYO9A* (Hom) *MAP3K8* (Hom) ADAMTSL3 (Hom) *RYR1* (3 CHZ) *ZNF862* (2 Hom) *CSPP1* (Hom) *CHRNB4* (Hom) *ZNF655* (Hom)

Filters applied exclude variants present in > 1% of the control population (ExAC database) and those that are not predicted to significantly impact protein structure and function (low and very low impact). Manual inspection includes the analysis of read depth, alignment of reads and quality of variants. The remaining variants are then subject to segregation analysis with family members. CHZ = compound heterozygous; Hom = homozygous.

MYO9A was therefore prioritized as the best candidate based on expression in muscle and nerve, and a function that could be consistent with causing CMS.

The *MYO9A* variants cause missense changes in highly conserved regions of the protein: one variant (rs149046541) is in exon 25 of the main transcript, which results in p.R1517H, and has a minor allele frequency (MAF) of 0.09% in the ExAC database. The other is in exon 40, rs142345927, which results in p.R2283H with a MAF of 0.2% in the ExAC database. The variants both reside in the tail domain: p.R1517H is located in a coiled coil region between an IQ motif and a protein kinase c domain and p.R2283H is located towards the N-terminus, adjacent to the Rho-GTPase domain (Fig. 1A). Both variants are predicted to be damaging by *in silico* variant effect prediction software (Schwarz *et al.*, 2014). Screening of whole-exome sequencing data from 277 patients, 50 of whom had a clinical diagnosis of CMS, identified another variant in *MYO9A* in CMS Patients 2 and 3 that segregates with the disease. The variant, rs150726107, which results in p.D1698G, has a MAF of 0.06% in the ExAC database. This variant is homozygous in this sib-pair, with parents both heterozygous for the variant as confirmed by Sanger sequencing. p.D1698G substitutes a highly conserved aspartic acid residue for glycine, again in the region between the IQ motif and the protein kinase C domain of the tail. Splicing prediction algorithms also indicate that this variant may introduce a new splice site or alter a splice enhancer site (Desmet *et al.*, 2009).

Remaining variants that co-segregate with the disease in Patients 2 and 3 are shown in Table 1. Variants in *MAP3K8*, *ADAMTSL3*, *ZNF862*, *ZNF655* and *CHRNB4* were excluded based on functions unrelated to CMS following a literature search. Mutations in *RYR1* are associated with malignant hyperthermia and congenital myopathies (Snoeck *et al.*, 2015). The variant identified in *CSPP1* has previously been reported in a patient with Joubert syndrome; however, we believe that the phenotype of our patients is not consistent with this disorder, including the defining feature of vermis cerebellar hypoplasia, lack of seizures and other CNS or cerebellar ataxia symptoms (Tuz *et al.*, 2014). In addition, *MYO9A* is the only gene shared between the two unrelated families with mutations that conform to the predefined filtering criteria.

MYO9A is expressed at the neuromuscular junction in mouse

To assess whether MYO9A is expressed at the NMJ in mammals we stained mouse lumbrical muscle using antibodies for MYO9A, synaptophysin and α-bungarotoxin. The use of the distal hind-limb lumbrical muscles for visualization of the NMJ allows for whole mount staining and gives an uninterrupted view of the NMJ (Sleigh *et al.*, 2014). The pattern of synaptophysin and acetylcholine receptor (AChR) immunoreactivity was consistent with previous reports (Sleigh *et al.*, 2014), labelling the presynaptic and postsynaptic regions of the NMJ, respectively (Wiedenmann and Franke, 1985; Brent and Drapeau, 2002). MYO9A staining co-localized with both markers, confirming expression of this unconventional myosin at the NMJ (Fig. 2).

Knockdown of MYO9A in NSC-34 cells affects neurite extension and branching

To assess whether MYO9A is involved in the morphology or sprouting of nerve cells, we knocked down MYO9A in

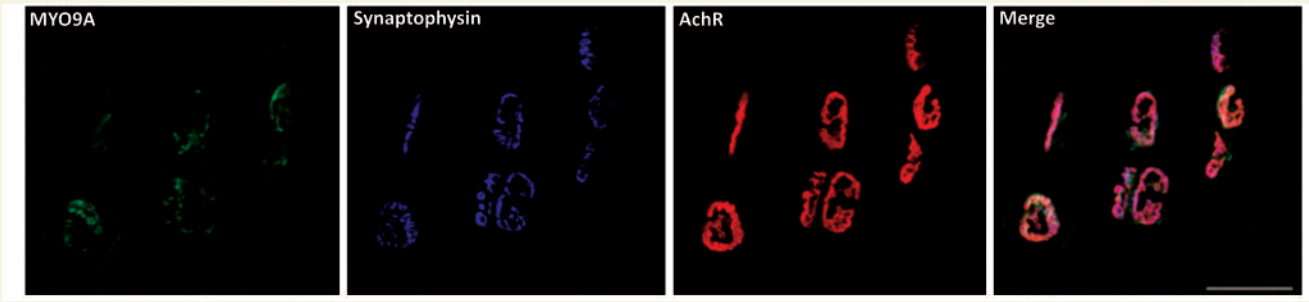

Figure 2 MYO9A is expressed at the mouse neuromuscular junction. MYO9A (green) co-localizes with Synaptophysin (blue) and acetylcholine receptor (AChR) clusters (α-bungarotoxin, red) in mouse whole lumbrical muscle mounts. Scale bar = 50 μm.

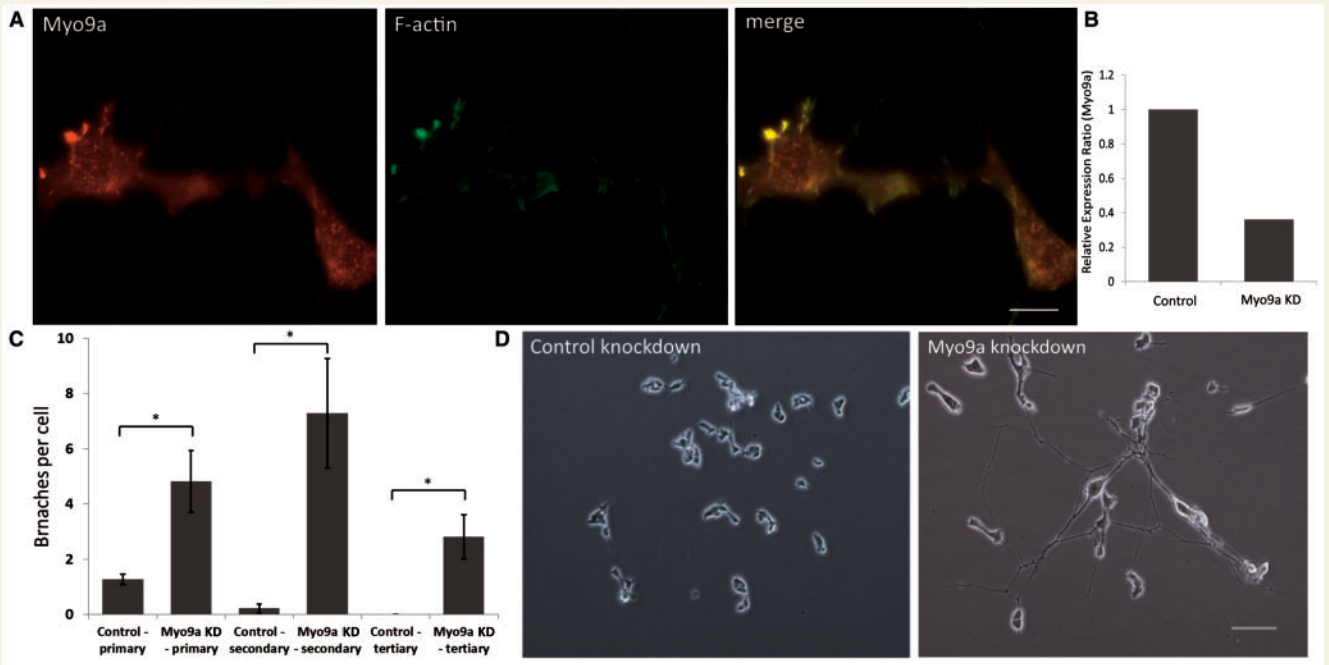

Figure 3 Knockdown of MYO9A in NSC-34 cells causes increased length and branching of neurites. (**A**) MYO9A (red) co-localizes with F-actin (phalloidin, green) at the growth cones of mouse derived NSC-34 cells. (**B**) Relative expression ratio of quantitative RT-PCR showing the expression of *Myo9a* mRNA in control cells and in MYO9A shRNA-mediated knockdown cells (NSC-34). A 6.4-fold decrease in *Myo9a* expression is observed. (**C**) Number of primary, secondary and tertiary branches of control and MYO9A knockdown cells (two-sample *t*-test, $*P < 0.05$). Graph depicts mean ± standard error of the mean (SEM). (**D**) Knockdown of MYO9A in NSC-34 cells leads to aberrant neurite length and branching as compared to control cells. Scale bar = 100 μm.

the mouse motor neuron derived cell line, NSC-34, following confirmation of MYO9A expression by western blotting (data not shown). Immunofluorescent staining of NSC-34 cells revealed a punctate staining pattern, with an accumulation at the growth cone of sprouting neurites, indicated by actin-rich filopodia stained with phalloidin (Fig. 3A). Immunofluorescent staining of C2C12 myotubes revealed no specific staining for MYO9A (data not shown).

Depletion of MYO9A from NSC-34 cells was confirmed by qRT-PCR (Fig. 3B), and revealed a significant increase in the number of primary, secondary and tertiary branches of the neurons (Fig. 3C and D; 10 fields of view measured per condition, $P < 0.05$). The average number of primary branches increased significantly from 1.27 per cell in control luciferase knockdowns to 4.82 per cell in MYO9A knockdowns ($P = 0.02$, two-sample *t*-test). Secondary branching rose from 0.22 per control cell to 7.29 in MYO9A knockdowns ($P = 0.011$, two-sample *t*-test) and tertiary branching increased from 0 to 2.81 ($P = 0.012$, two-sample *t*-test). There was also a significant increase in the average length of neurite extensions of 208% ($P < 0.001$, two-sample *t*-test). The average length of neurite extensions from control cells was 55.8 μm whereas the MYO9A knockouts had an average length of 116.1 μm (Fig. 3D).

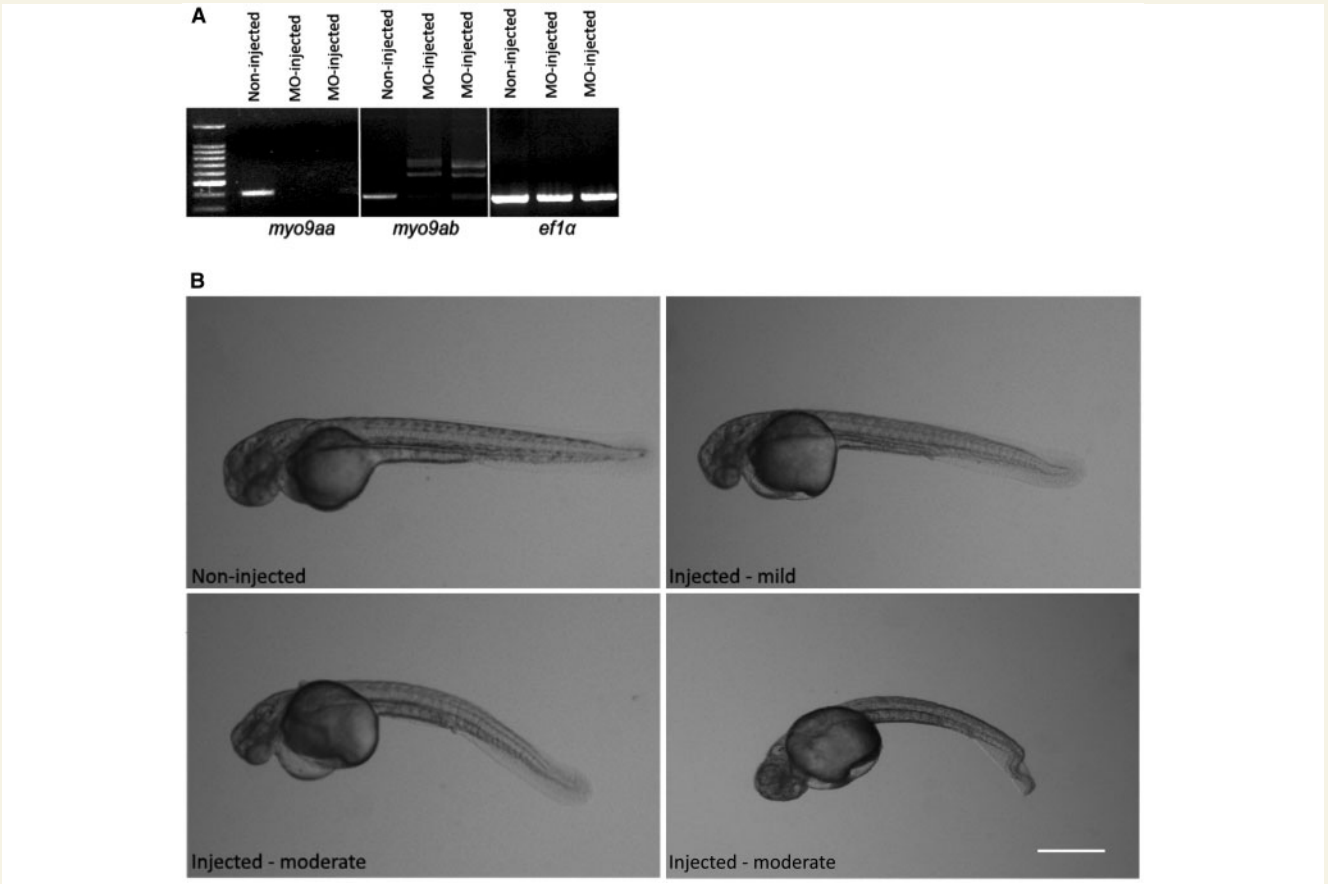

Figure 4 Knockdown of MYO9A in zebrafish. (**A**) RT-PCR confirming knockdown success of *myo9aa* and *myo9ab* in zebrafish injected with morpholino oligonucleotide. There is loss of the *myo9aa* transcript and an alternatively spliced *myo9ab* transcript produced due to intron retention. Bands from the same gel have been cropped and put together for comparison, demarcated by the white lines. (**B**) Images of non-injected and mild/moderate *myo9aa/ab* morpholino oligonucleotide-injected zebrafish (48 hpf), with the latter displaying varying severities of tail curvature. Scale bar = 100 μm.

Knockdown of MYO9A in zebrafish affects tail morphology and causes abnormal movement

Two *MYO9A* orthologues were identified in zebrafish, *myo9aa and myo9ab*, as shown in Supplementary Fig. 2, and knockdown was confirmed by reverse transcriptase PCR (Fig. 4A). The same phenotype, characterized by curly tails and abnormal swimming in response to tactile stimulation, was seen in both *myo9aa* and *myo9ab* morphants but not in non-injected, control morpholino injected or *p53* morpholino oligonucleotide injected embryos (Supplementary Fig. 3) (Robu *et al.*, 2007). The morpholino oligonucleotides were then co-injected, along with the *p53* morpholino oligonucleotide to help reduce non-specific effects. The *myo9aa/myo9ab* morphants displayed a pronounced phenotype at 48 hpf following dechorionation, including varying severities of tail curvature (Fig. 4B), abnormal swimming and cardiac oedema, which was not alleviated by the *p53* morpholino oligonucleotide.

At 17 hpf the embryos perform slow alternating movements spontaneously in the chorion, encompassing the first stage of locomotor development in the zebrafish (Saint-Amant and Drapeau, 1998). Morphants moved significantly less within 10 s than non-injected embryos ($P = 0.025$, two-sample *t*-test), with morphants twisting their tails only 0.5 times on average as opposed to the 0.95 times performed by control fish (20 embryos observed from each condition, Supplementary Videos 1–8). The normal response of zebrafish at 48 hpf to tactile stimulation is to swim rapidly away by at least one body length (Saint-Amant and Drapeau, 1998). However, *myo9aa/myo9ab* knockdowns in some cases did not respond at all, and in others were only able to twitch or swim in circles (Supplementary Videos 9 and 10).

To determine whether the abnormalities observed in the morphant zebrafish in response to tactile stimulation were due to a sensory or CNS defect, rather than faulty NMJ transmission, islet-1 transgenic zebrafish were also injected with the *myo9aa/ab/p53* morpholino oligonucleotides. Downregulation of both orthologues revealed no changes to the cranial motor neurons (Supplementary Fig. 4A and B) or the Rohon Beard primitive sensory cells (Nüsslein-Volhard and Dahm, 2002), suggesting that a lack of

sensory transmission is not the cause of the abnormal movement observed.

MYO9A knockdown affects motor neuron guidance in zebrafish

The formation of the neuromuscular junction in zebrafish begins with the distribution of pre-patterned AChR clusters (Flanagan-Steet et al., 2005) followed by the outgrowth of primary motor neurons. The contact of a motor neuron causes the integration and stabilization of the aneural AChR clusters to form NMJs. There is usually a tight juxtaposition of the presynaptic and postsynaptic regions, as evidenced by staining of presynaptic proteins such as synaptic vesicle protein 2 (SV2, encoded by *SV2A*) (Buckley and Kelly 1985) and α-bungarotoxin, which specifically labels the postsynaptic AChRs (Brent and Drapeau 2002). In *myo9aa/ab* morphants, axons are aberrant, either shortened or over-extended, with some axons appearing to branch to the adjacent myotome (Fig. 5).

Discussion

Our data provide support for a novel CMS gene: *MYO9A*, identified by whole-exome sequencing in two unrelated families. Diagnosis of CMS can often be problematic as it manifests with a broad spectrum of symptoms and subtypes of CMS are difficult to differentiate only on clinical grounds often requiring genetic testing either by Sanger sequencing or more recently through whole-exome sequencing (Chae *et al.*, 2015). Whole-exome sequencing has also proven to be a successful method in the identification of novel CMS-causing genes that are not obviously associated with NMJ function, such as the ubiquitously expressed glycosylation pathway proteins DPAGT (*DPAGT1*) and GMPPB (Belaya *et al.*, 2012, 2015).

The variants identified in this study highlight a new avenue of proteins that may be involved in the NMJ function, the unconventional myosins. A recent publication has identified *MYO9A* mutations in a patient presenting with arthrogryposis (Bayram *et al.*, 2016). Overlapping phenotypes and association to the same causative genes have been described previously for arthrogryposis and CMS, with joint contractures (arthrogryposis) developing due to reduced foetal movements based on antenatal neuromuscular transmission defects (Vajsar *et al.*, 1995; Brownlow *et al.*, 2001). The prevalence of p.R2283H at 0.2%, with a predicted homozygote frequency of 4 in 1 000 000 is higher than might be expected in CMS. We hypothesize that p.R2283H has a relatively mild effect on protein structure, with subclinical manifestations when found in homozygosis; however, it has sufficient effect on the protein to cause disease when coupled with the rarer p.R1517H that affects a coiled coil region of MYO9A. Interestingly, the *MYO9A* mutation described by Bayram *et al.* (2016) results in p.G2282E, affecting the neighbouring residue of our p.R2283H variant. The possibility remains that p.D1698G could be a population-enriched variant; however, due to the lack of any large Kurdish control cohorts the carrier frequency of this variant is difficult to assess.

The findings presented from both *in vitro* and *in vivo* investigations provide support for the presence of MYO9A at the NMJ. However, the exact location of MYO9A at the human NMJ has not been determined and conclusive evidence for the presynaptic nature of the CMS in our patients has not been obtained. Our mouse muscle immunofluorescence data demonstrate, however, a co-localization of MYO9A with the NMJ in muscle whole mounts. There is also an enrichment of MYO9A at the growth cones of NSC-34 cells, suggesting MYO9A may have presynaptic involvement. Other unconventional myosins with a similar structure to MYO9A, such as

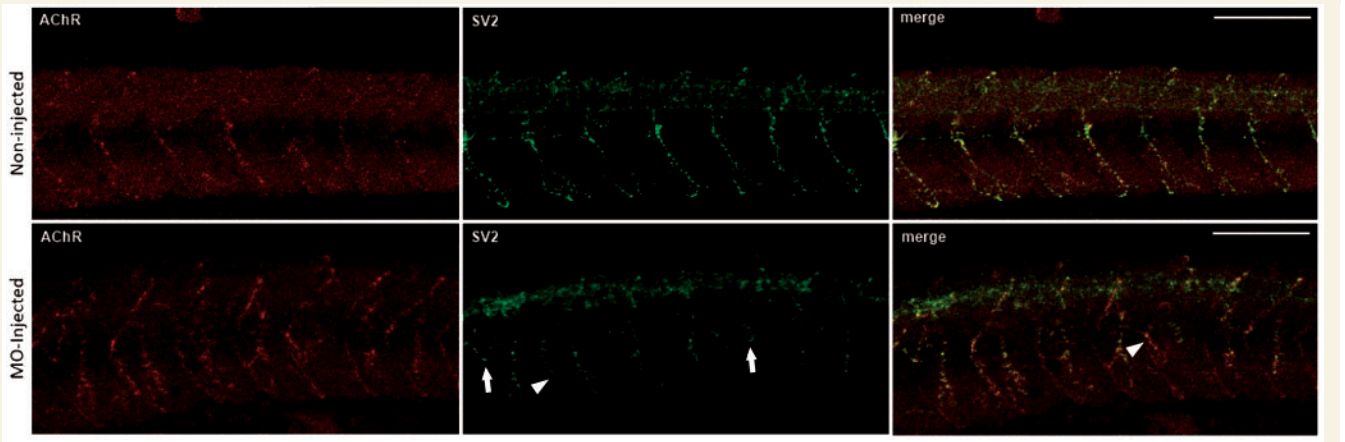

Figure 5 Motor axons of morphant zebrafish are shortened and abnormally branched. Neuromuscular junctions in absence of Myo9aa/ab. Non-injected and *myo9aa/ab* morpholino oligonucleotide-injected embryos were stained for presynaptic motor axons (SV2, green) and postsynaptic AChRs (α-bungarotoxin, red) at 48 hpf. Morphant zebrafish display shortened (arrow) and abnormally branched motor axons, with some innervating adjacent myotomes (arrowhead). Scale bar = 100 μm.

MYO10 and MYO5, have also been associated with the growth cones of neurons (Suter *et al.*, 2000; Yu *et al.*, 2015). MYO5, like MYO9A, is present in the cell body, neurites and growth cones of neuronal cells (Suter *et al.*, 2000) and has been implicated in actin-based organelle transport in growth cones (Huang *et al.*, 1999). MYO10 is involved in filopodia extension and cell motility, with deficiency in MYO10 leading to excessive extension of neurites (Yu *et al.*, 2015). To determine whether MYO9A is actively involved in the growth cone dynamics we analysed MYO9A knockdown NSC-34 cells. This similarly revealed an increase in branch count and length of sprouting neurites. This change in morphology observed in the motor neuron cell line was also reflected in the zebrafish morphants, in which axon guidance and branching was disrupted and some axons extended beyond their target to innervate adjacent myotomes.

In the mouse model (Thelen *et al.*, 2015), loss of MYO9A in the kidney led to a dysregulation of endocytosis, a process crucial for the uptake of activated growth signal receptors in migrating neurons. Defects in endocytosis may prevent an appropriate response of motor neurons to guidance cues, an outcome potentially observed in Myo9aa/ab deficient zebrafish. This cellular function is also important for synaptic recycling at the NMJ, and failings here may prevent efficient repackaging of acetylcholine into vesicles for release (Ceccarelli *et al.*, 1973). Delay in acetylcholine release is also affected in patients with choline acetyltransferase CMS, who present with a similar phenotype to our patients (Ohno *et al.*, 2001).

Zebrafish NMJs are extremely useful model systems (Babin *et al.*, 2014), as they are highly homologous to the mammalian NMJ and development begins when the embryo is transparent and can be easily manipulated. Our zebrafish data indicate that Myo9aa/ab are required for the formation of appropriate non-focal and focal innervations as the presynaptic motor neurons of the morphant fish fail to form typical contacts across the myotome. The morphological changes observed are reflected functionally, with a lack of Myo9aa/ab affecting both the spontaneous movement and response to tactile stimulation stages of locomotor development, suggestive of an NMJ transmission defect. If morpholino oligonucleotide knockdown caused developmental delay, shortening of axons at the caudal end of the tail would be expected; however, motor axons in the morphant fish were affected throughout the tail suggesting loss of Myo9aa/ab did not simply slow development. Presence of a peripheral motor defect was reaffirmed by the assessment of islet-1 fish and intriguingly the MYO9A knockout mouse also revealed movement abnormalities of a hopping and trembling gait (Abouhamed *et al.*, 2009), with abnormal gait also being a feature in other mouse models of CMS such as those affected by MuSK mutations, as well as in mice with presynaptic motor defects (Chevessier *et al.*, 2008; Dale *et al.*, 2012). The *Myo9a* null mice also have hydrocephalus, whereas brain abnormalities were not present in the zebrafish, the *Myo9a* heterozygous knockout mice (Abouhamed *et al.*, 2009) or our patients. However, the missense variants identified here and the gene knockdown in zebrafish do not represent a full knockout situation as seen in the homozygous knockout mice, but rather hypomorphic alleles that may provide sufficient MYO9A function to rescue any brain abnormalities.

We conclude that the unconventional myosin MYO9A is expressed and functional at the mammalian NMJ, and recessive missense variants of the *MYO9A* gene are associated with CMS in two families. While not fully conclusive of presynaptic form of CMS, the phenotype of the patients, such as the severe neonatal onset with respiratory distress and bulbar involvement, and the experimental data obtained in different models are consistent with a presynaptic defect (Palace and Beeson, 2008; Eymard *et al.*, 2013). There are relatively few forms of presynaptic CMS that have been described to date (Ohno *et al.*, 2001; Chaouch *et al.*, 2014; Herrmann *et al.*, 2014), and no mutations in genes encoding proteins that affect the structure of the presynaptic NMJ have been described. Our data regarding the function of MYO9A *in vitro* and *in vivo*, however, suggest a potential role in the structural integrity of the peripheral nerve terminal.

Acknowledgements

Andreas Roos, Rita Barresi, Matthew Henderson, Rolf Stucka, Marina Dusl, Velina Guergueltcheva and Brunhilde Wirth provided critical discussion and logistical support.

Funding

The study was supported by the Medical Research Council UK (reference G1002274, grant ID 98482), by the European Union Seventh Framework Programme (FP7/2007-2013) under grant agreement No. 305444 (RD-Connect) and 305121 (NeurOmics). The authors also acknowledge support from the NeurOmics consortium and deCODE genetics.

Supplementary material

Supplementary material is available at *Brain* online.

References

Abouhamed M, Grobe K, San IV, Thelen S, Honnert U, Balda MS, et al. Myosin IXa regulates epithelial differentiation and its deficiency results in hydrocephalus. Mol Biol Cell 2009; 20: 5074–85.

Babin PJ, Goizet C, Raldua, D. Zebrafish models of human motor neuron diseases: advantages and limitations. Prog Neurobiol 2014; 118: 36–58.

Bayram Y, Karaca E, Coban Akdemir Z, Yilmaz E O, Tayfun G A, Aydin H, et al. Molecular etiology of arthrogryposis in multiple families of mostly Turkish origin. J Clin Invest 2016; 126: 762–78.

Belaya K, Finlayson S, Cossins J, Liu WW, Maxwell S, Palace J, et al. Identification of DPAGT1 as a new gene in which mutations cause a congenital myasthenic syndrome. Ann N Y Acad Sci 2012; 1275: 29–35.

Belaya K, Rodriguez Cruz P M, Liu WW, Maxwell S, McGowan S, Farrugia ME, et al. Mutations in GMPPB cause congenital myasthenic syndrome and bridge myasthenic disorders with dystroglycanopathies. Brain 2015; 138: 2493–504.

Brent LJ, Drapeau P. Targeted "knockdown" of channel expression in vivo with an antisense morpholino oligonucleotide. Neuroscience 2002; 114: 275–8.

Bridgman PC. Myosin motor proteins in the cell biology of axons and other neuronal compartments. Results Probl Cell Differ 2009; 48: 91–105.

Brownlow S, Webster R, Croxen R, Brydson M, Neville B, Lin JP, et al. Acetylcholine receptor delta subunit mutations underlie a fast-channel myasthenic syndrome and arthrogryposis multiplex congenita. J Clin Invest 2001; 108: 125–30.

Buckley K, Kelly RB. Identification of a transmembrane glycoprotein specific for secretory vesicles of neural and endocrine cells. J Cell Biol 1985; 100: 1284–94.

Ceccarelli B, Hurlbut WP, Mauro A. Turnover of transmitter and synaptic vesicles at the frog neuromuscular junction. J Cell Biol 1973; 57: 499–524.

Chae JH, Vasta V, Cho A, Lim BC, Zhang Q, Eun SH, et al. Utility of next generation sequencing in genetic diagnosis of early onset neuromuscular disorders. J Med Genet 2015; 52: 208–16.

Chaouch A, Porcelli V, Cox D, Edvardson S, Scarcia P, Grassi AD, et al. Mutations in the mitochondrial citrate carrier SLC25A1 are associated with impaired neuromuscular transmission. J Neuromuscul Dis 2014; 1: 75–90.

Chevessier F, Girard E, Molgo J, Bartling S, Koenig J, Hantai D, et al. A mouse model for congenital myasthenic syndrome due to MuSK mutations reveals defects in structure and function of neuromuscular junctions. Hum Mol Genet 2008; 17: 3577–95.

Cruz PM, Palace J, Beeson D. Congenital myasthenic syndromes and the neuromuscular junction. Curr Opin Neurol 2014; 27: 566–75.

Dale JM, Villalon E, Shannon SG, Barry DM, Markey RM, Garcia VB, et al. Expressing hNF-LE397K results in abnormal gaiting in a transgenic model of CMT2E. Genes Brain Behav 2012; 11: 360–5.

Desmet FO, Hamroun D, Lalande M, Collod-Beroud G, Claustres M, Beroud C. Human splicing finder: an online bioinformatics tool to predict splicing signals. Nucleic Acids Res 2009; 37: 67.

ExAC database. Exome Aggregation Consortium (ExAC). Cambridge, MA. Available from: http://exac.broadinstitute.org. (May 2015, date last accessed).

Eymard B, Hantai D, Estournet B. Congenital myasthenic syndromes. Handb Clin Neurol 2013; 113: 1469–80.

Finlayson S, Beeson D, Palace J, Congenital myasthenic syndromes: an update. Pract Neurol 2013; 13: 80–91.

Flanagan-Steet H, Fox MA, Meyer D, Sanes JR. Neuromuscular synapses can form in vivo by incorporation of initially aneural postsynaptic specializations. Development 2005; 132: 4471–81.

Hartman MA, Finan D, Sivaramakrishnan S, Spudich JA. Principles of unconventional myosin function and targeting. Annu Rev Cell Dev Biol 2011; 27: 133–55.

Herrmann DN, Horvath R, Sowden JE, Gonzalez M, Sanchez-Mejias A, Guan Z, et al. Synaptotagmin 2 mutations cause an autosomal-dominant form of lambert-eaton myasthenic syndrome and nonprogressive motor neuropathy. Am J Hum Genet 2014; 95: 332–9.

Higashijima S, Hotta Y, Okamoto H. Visualization of cranial motor neurons in live transgenic zebrafish expressing green fluorescent protein under the control of the islet-1 promoter/enhancer. J Neurosci 2000; 20: 206–18.

Huang JD, Brady ST, Richards BW, Stenolen D, Resau JH, Copeland NG, et al. Direct interaction of microtubule- and actin-based transport motors. Nature 1999; 397: 267–70.

Kent WJ, Sugnet CW, Furey TS, Roskin KM, Pringle TH, Zahler AM, et al. The human genome browser at UCSC. Genome Res 2002; 12: 996–1006.

Liao W, Elfrink K, Bahler M. Head of myosin IX binds calmodulin and moves processively toward the plus-end of actin filaments. J Biol Chem 2010; 285: 24933–42.

Muller JS, Jepson CD, Laval SH, Bushby K, Straub V, Lochmuller H. Dok-7 promotes slow muscle integrity as well as neuromuscular junction formation in a zebrafish model of congenital myasthenic syndromes. Hum Mol Genet 2010; 19: 1726–40.

Nüsslein-Volhard C, Dahm R. Zebrafish: a practical approach. The practical approach series. 1st edn. Oxford: Oxford University Press; 2002.

Ohno K, Tsujino A, Brengman JM, Harper CM, Bajzer Z, Udd B, et al. Choline acetyltransferase mutations cause myasthenic syndrome associated with episodic apnea in humans. Proc Natl Acad Sci USA 2001; 98: 2017–22.

Omelchenko T. Regulation of collective cell migration by RhoGAP myosin IXA. Small GTPases 2012; 3: 213–18.

Palace J, Beeson D. The congenital myasthenic syndromes. J Neuroimmunol 2008; 201–202: 202–5.

Pastural E, Barrat FJ, DufourcqLagelouse R, Certain S, Sanal O, Jabado N, et al. Griscelli disease maps to chromosome 15q21 and is associated with mutations in the myosin-Va gene. Nat Genet 1997; 16: 289–92.

Pruitt KD, Brown GR, Hiatt SM, Thibaud-Nissen F, Astashyn A, Ermolaeva O, et al. RefSeq: an update on mammalian reference sequences. Nucleic Acids Res 2014; 42: 756–63.

Robu ME, Larson JD, Nasevicius A, Beiraghi S, Brenner C, Farber SA, et al. p53 activation by knockdown technologies. PLoS Genet 2007; 3: 78.

Ryan CL, Baranowski DC, Chitramuthu BP, Malik S, Li Z, Cao M, et al. Progranulin is expressed within motor neurons and promotes neuronal cell survival. BMC Neurosci 2009; 10: 130.

Saint-Amant L, Drapeau P. Time course of the development of motor behaviors in the zebrafish embryo. J Neurobiol 1998; 37: 622–32.

Schwarz JM, Cooper DN, Schuelke M, Seelow D. MutationTaster2: mutation prediction for the deep-sequencing age. Nat Methods 2014; 11: 361–2.

Sleigh JN, Burgess RW, Gillingwater TH, Cader MZ. Morphological analysis of neuromuscular junction development and degeneration in rodent lumbrical muscles. J Neurosci Methods 2014; 227: 159–65.

Snoeck M, van Engelen BG, Kusters B, Lammens M, Meijer R, Molenaar JP, et al. RYR1-related myopathies: a wide spectrum of phenotypes throughout life. Eur J Neurol 2015: 22: 1094–112.

Suter DM, Espindola FS, Lin CH, Forscher P, Mooseker MS. Localization of unconventional myosins V and VI in neuronal growth cones. J Neurobiol 2000; 42: 370–82.

Thelen S, Abouhamed M, Ciarimboli G, Edemir B, Bahler M. The Rho GAP Myosin IXa is a regulator of kidney tubule function. Am J Physiol Renal Physiol 2015; 309: 501–13.

Tuz K, Bachmann-Gagescu R, O'Day DR, Hua K, Isabella CR, Phelps IG, et al. Mutations in CSPP1 cause primary cilia abnormalities and joubert syndrome with or without jeune asphyxiating thoracic dystrophy. Am J Hum Genet 2014; 94: 62–72.

Vajsar J, Sloane A, Macgregor DL, Ronen GM, Becker LE, Jay V. Arthrogryposis multiplex congenita due to congenital myasthenic syndrome. Pediatr Neurol 1995; 12: 237–41.

Well D, Blanchard S, Kaplan J, Guilford P, Gibson F, Walsh J, et al. defective myosin viia gene responsible for usher syndrome type 1b. Nature 1995; 374: 60–1.

Wiedenmann B, Franke WW. Identification and localization of synaptophysin, an integral membrane glycoprotein of Mr 38,000 characteristic of presynaptic vesicles. Cell 1985; 41: 1017–28.

Yu H, Sun D, Wang N, Wang M, Lan Y, Fan W, et al. Headless Myo10 is a regulator of microtubule stability during neuronal development. J Neurochem 2015; 135: 261–73.

Zhu XJ, Wang CZ, Dai PG, Xie Y, Song NN, Liu Y, et al. Myosin X regulates netrin receptors and functions in axonal path-finding. Nat Cell Biol 2007; 9: 184–92.